Journal of Medicinal Chemistry

ARTICLE

pubs.acs.org/jmc

Development of Indole Compounds as Small Molecule Fusion Inhibitors Targeting HIV-1 Glycoprotein-41

Guangyan Zhou,*[,†] Dong Wu,[†] Beth Snyder,[‡] Roger G. Ptak,[‡] Harmeet Kaur,[†] and Miriam Gochin*[,†,§]

[†]Department of Basic Sciences, Touro University—California, 1310 Club Drive, Mare Island, Vallejo, California 94592, United States

[‡]Southern Research Institute, 431 Aviation Way, Frederick, Maryland 21701, United States

[§]Department of Pharmaceutical Chemistry, University of California San Francisco, California 94143, United States

Supporting Information

ABSTRACT: Nonpeptide inhibition of fusion remains an important goal in anti-HIV research, due to its potential for low cost prophylaxis or prevention of cell−cell transmission of the virus. We report here on a series of indole compounds that have been identified as fusion inhibitors of gp41 through a structure-based drug design approach. Experimental binding affinities of the compounds for the hydrophobic pocket were strongly correlated to fusion inhibitory data (R^2 = 0.91), and corresponding inhibition of viral replication confirmed the hydrophobic pocket as a valid target for low molecular weight fusion inhibitors. The most active compound bound to the hydrophobic pocket and inhibited cell−cell fusion and viral replication at submicromolar levels. A common binding mode for the inhibitors in this series was established by carrying out docking studies using structures of gp41 in the Protein Data Bank. The molecules were flexible enough to conform to the contours of the pocket, and the most active compound was able to adopt a structure mimicking the hydrophobic contacts of the D-peptide PIE7. The results enhance our understanding of indole compounds as inhibitors of gp41.

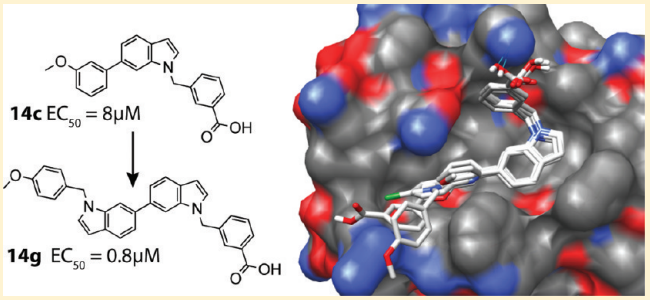

INTRODUCTION

The continued HIV/AIDS epidemic worldwide and the absence of a vaccine to counter the spread of infection have sparked the development of an ever-expanding repertoire of anti-HIV drugs. New classes of drugs acting with a novel mechanism continue to be advantageous, due to the appearance of resistance to drugs used in the clinic. Entry inhibitors are of particular interest, since they could be used therapeutically to prevent the spread of infection among cells or in prophylactic form to prevent transmission of the virus between individuals. Small molecule fusion inhibitors acting on conserved elements of the HIV-1 envelope glycoprotein gp41 are promising in this regard, since gp41 is universally required by all HIV strains. Gp41 facilitates the viral fusion process through a conformational switch involving association of three C-heptad repeat (CHR) helices along the conserved hydrophobic grooves of a central trimeric N-heptad repeat (NHR) coiled coil.[1−3] Many studies indicate that a fairly long-lived intermediate exists in which the coiled coil is exposed and susceptible as a drug target. However, the only currently available highly active fusion inhibitors targeting gp41 are peptides, including enfuvirtide (T20), a 36 amino acid peptide that was derived from the CHR and approved by the Food and Drug Administration (FDA) in 2003,[4] and D-peptide inhibitors, which target a known hydrophobic pocket on the coiled coil revealed by crystal structures.[5−8] Because of the lack of oral availability, emergence of drug resistance, and high cost of enfuvirtide, small molecule inhibitors of gp41 are highly desirable.

The hydrophobic pocket is critical for the stability of the six-helix bundle (6-HB) and is considered a hotspot for small molecule drug design. It can accommodate a compound with a molecular mass of 500−600 Da.[9] Several studies have been carried out to identify small molecule compounds that target this pocket. These molecules include α-helical peptidomimetic compounds with ∼15 μM effective concentration for 50% inhibition (EC_{50}) against HIV fusion,[10] a series of phenylpyrroles[11−14] and furan derivatives[15,16] with low to midmicromolar EC_{50} antifusion activity and low nanomolar antiviral activity, and several other compounds with antifusion activity in the tens of micromolar.[17,18]

All known small molecule inhibitors have demonstrated no better than several micromolar inhibition of fusion, which represents a significant challenge to small molecule drug discovery against this target. It is compounded by the fact that no crystal structure of gp41 with a small molecule has been reported. Only recently, three NMR structures with weakly bound ligands have been obtained.[19−21] Most known small molecule inhibitors of gp41 have been identified by screening typical small molecule libraries, which may not be sufficient for harvesting compounds

Received: June 18, 2011
Published: September 19, 2011

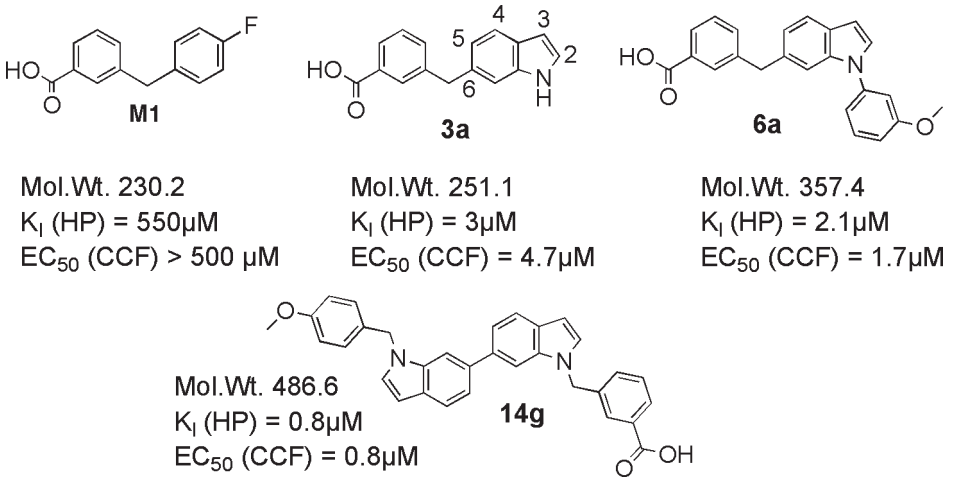

Figure 1. Structure and activity data of indole inhibitors in the lead optimization progression.

Scheme 1

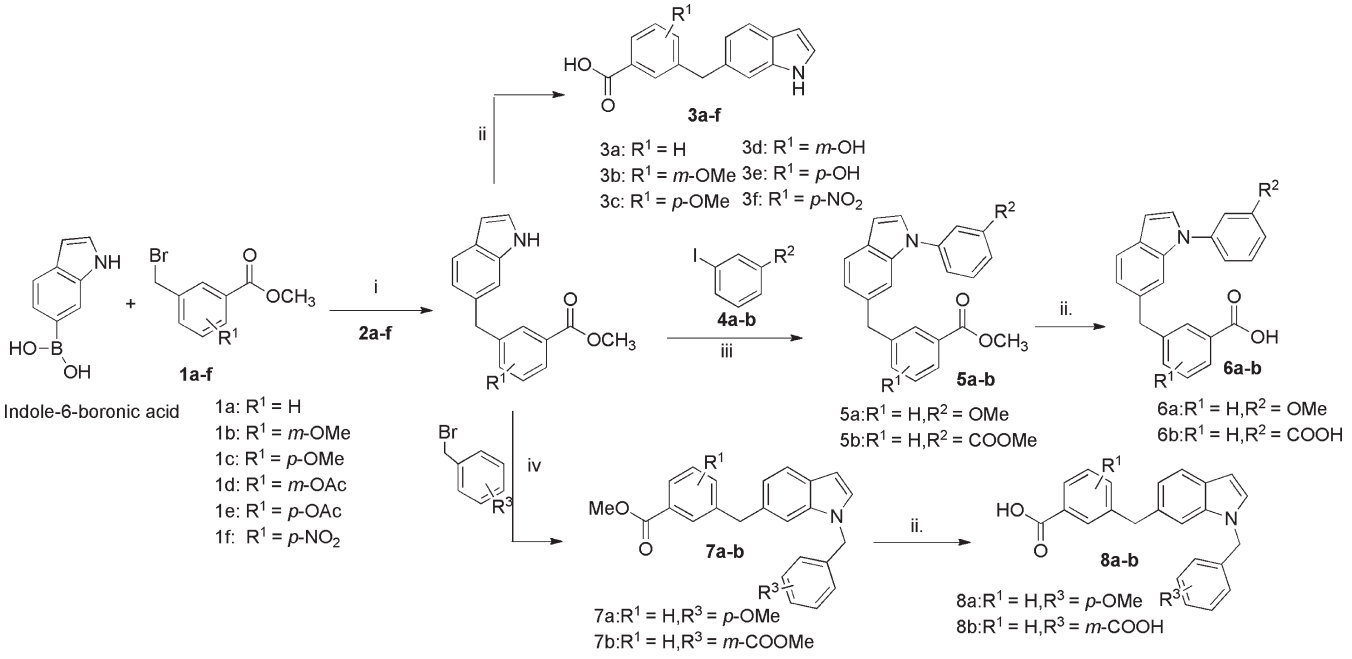

that block the protein−protein interaction between the NHR and the CHR of gp41. Most of the chemical entities in standard libraries have been generated for classical medicinal targets.[22]

We have previously reported eight indole compounds as inhibitors targeting the hydrophobic pocket with mid to low micromolar EC_{50} values against HIV fusion.[23] These compounds were designed from an NMR structural study of a weakly bound inhibitor **M1** (Figure 1) in the hydrophobic pocket.[20,23] Compounds **3a** and **6a** (Figure 1) were described in the previous study. The optimization process described here has yielded compound **14g**, with an extended structure more typical of a protein−protein interaction inhibitor, and with submicromolar hydrophobic pocket binding affinity and inhibitory activity against cell−cell fusion (CCF) and viral replication. It is the first verified low molecular weight fusion inhibitor with <1 μM 50% inhibitory concentration. We report our lead optimization process and potential binding modes in the pocket. Overlapping binding poses of inhibitors of increased length suggested that they could adjust to the contours of the hydrophobic pocket and mimic interactions typically seen with peptide inhibitors. Calculated poses gave a good prediction of observed rank order, with the exception of compounds with two polar ends.

RESULTS AND DISCUSSION

The strategy for lead optimization was as follows: (1) retain the COOH group, which was confirmed to be essential for binding; (2) extend the length of the compound as is generally required to inhibit a protein−protein interaction; and (3) consider shape complementarity by designing inhibitors having flexible groups at both ends to adapt to the contours of the groove. In addition, modifications were made that could "fill out" the area occupied by the molecule in the main pocket. Six-substituted indole compounds are described in Schemes 1−3

dx.doi.org/10.1021/jm200791z |J. Med. Chem. 2011, 54, 7220–7231

Scheme 2

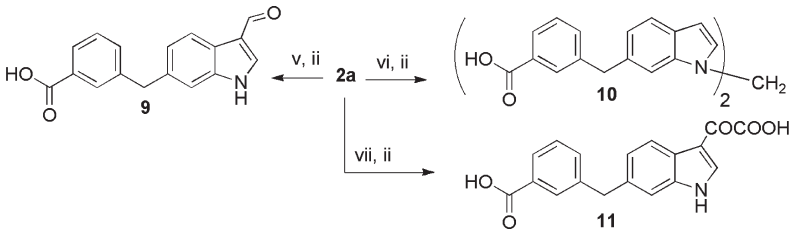

Scheme 3

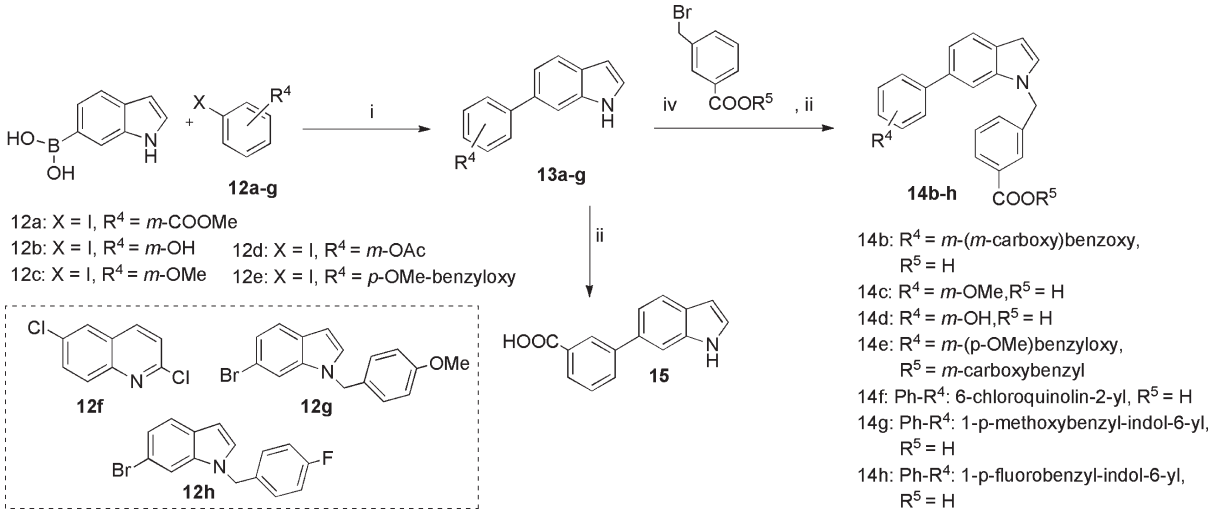

(see the Experimental Section). Three compounds with a 5-substituted indole were also prepared, namely, **3g**, **8c**, and **14i**. These compounds are isomers of 6-indole variants **3a**, **8b**, and **14f**, respectively (see the numbering in Figure 1 and the Supporting Information, Figure S1). Compounds were analyzed for biological activity in an assay for binding to the gp41 hydrophobic pocket,[24] in an HIV-1 HXB2 Env-mediated CCF assay[25] and in viral replication assays using HIV-1 Ba-L and HIV-1 IIIB;[26,27] examples are shown in Figure 2 and Figure S2 in the Supporting Information. Cell culture experiments were conducted at varying concentrations of serum, because of our discovery that serum blunts the effect of many of the compounds, proportionately increasing the EC_{50} values observed in fusion, viral replication, and cytotoxicity experiments (Table 1 and Table 2).

Lead Optimization. *Modification of Compounds with Two-Ring Systems.* The predicted orientation of small indole compounds in the pocket was based on early docking studies[23] as well as two NMR structures obtained on compound **M1**[20] and on **3g**,[21] the 5-substituted indole isomer of **3a**. The results indicated that the carboxylate group of the ligand pointed toward Lys574. This implies that the aromatic ring supporting the carboxylate lies in a strongly hydrophobic part of the pocket lined by residues Leu565′, Leu568′, Trp571′, and Val570. The bend provided by the CH_2 group between aromatic moieties was essential for shape complementarity, and absence of this hinge led to a 10-fold reduction in potency (compound **15**). Substitution on the benzyl ring of **3a** was studied to potentially improve affinity through (1)

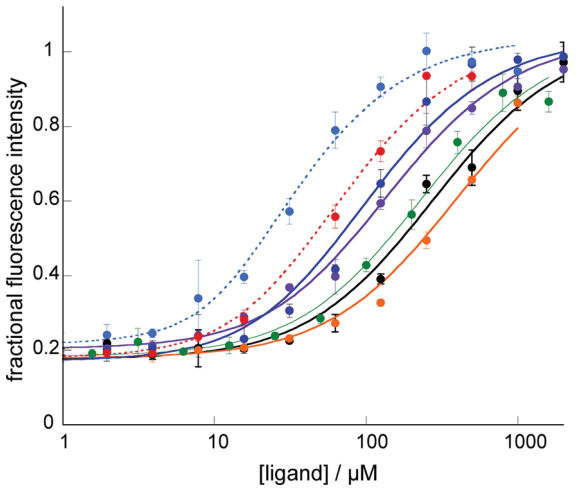

Figure 2. Typical competitive inhibition curves for indole inhibitors binding to the hydrophobic pocket. The fluorescence intensity of 15 nM probe peptide C18-FL was measured in the presence of 7.2 μM Fe(env2.0)$_3$ and varying concentrations of inhibitors, **3a** (gray), **3b** (dark blue), **3c** (green), **3d** (orange), **3e** (purple), **3f** (black), **8a** (red), and **14g** (light blue). Data are plotted relative to control values for C18-FL in the absence of Fe(env2.0)$_3$ and were fit to the equation: $F_{obs} = F_{RL} + 0.6 \times (1 - F_{min})/([R] + 0.6)$ where $[R] = 1/2\{7.2 - I_t - K_I + ((7.2 - I_t - K_I)^2 + 28.8K_I)^{1/2}\}$ to obtain the inhibition constant in μM.[24] F_{min} is a parameter representing the fractional fluorescence of the C18-FL−Fe(env2.0)$_3$ complex in the absence of inhibitor.

dx.doi.org/10.1021/jm200791z | J. Med. Chem. 2011, 54, 7220–7231

Table 1. Molecular Weight, Inhibition Constants, Fusion and Viral Inhibitory Activity, and Cytotoxicity of Indole Compounds in Series 3−11

compd	mol. wt.	cLog *P*	obs. K_I (μM)[a]	% serum	virus strain	EC_{50} (μM) CCF[b]	EC_{50} (μM) HIV-1 replication	CC_{50} (μM) cytotoxicity [b]
3a	251.1	3.30	3.5 ± 1.5	0	HXB2	4.7 ± 1		>500
				2	Ba-L		15.5	>100
				5			34.8	>100
				10			44.7	>100
				10	IIIB		100	>100
3b	280.3	3.19	9 ± 2	0	HXB2	18 ± 2		>100
				2	Ba-L		8.65	>100
				5			>100	>100
				10			>100	>100
				10	IIIB		>100	>100
3c	280.3	3.19	16 ± 3	0	HXB2	>100		>100
				2	Ba-L		>100	>100
				5			>100	>100
				10			>100	>100
				10	IIIB		>100	>100
3d	267.3	3.00	30 ± 4	0	HXB2	>100		>500
				2	Ba-L		>100	>100
				5			>100	>100
				10			>100	>100
				10	IIIB		>100	>100
3e	267.3	3.00	8 ± 2	0	HXB2	19 ± 2		>500
				2	Ba-L		42.7	>100
				5			89.3	>100
				10			>100	>100
				10	IIIB		>100	>100
3f	296.3	3.30	10 ± 2	0	HXB2	37 ± 3		>100
				2	Ba-L		18.5	>100
				5			82.7	>100
				10			>100	>100
				10	IIIB		>100	>100
3g	251.1	3.30	18 ± 5	0	HXB2	48 ± 4		>400
				2	Ba-L		42.4	>100
				5			52.4	>100
				10			63.5	>100
				10	IIIB		>100	>100
6a	357.4	4.48	2.1 ± 0.2	0	HXB2	1.7 ± 0.4		>100
				2	Ba-L		15.8	>100
				5			34	>100
				10			67.7	>100
				10	IIIB		61.5	>100
6b	371.4	4.11	45 ± 5	0	HXB2	186 ± 16		>400
8a	371.4	4.59	3.4 ± 1.1	0	HXB2	5.3 ± 1		100
				2	Ba-L		55.8	92.7
				5			91.2	>100
				10			>100	>100
				10	IIIB		>100	>100

dx.doi.org/10.1021/jm200791z |*J. Med. Chem.* 2011, 54, 7220–7231

Table 1. Continued

compd	mol. wt.	cLog *P*	obs. K_I (μM)[a]	% serum	virus strain	EC_{50} (μM) CCF[b]	EC_{50} (μM) HIV-1 replication	CC_{50} (μM) cytotoxicity [b]
8b	385.4	4.22	22 ± 2	0	HXB2	130 ± 5		>200
8c	385.4	4.22	35 ± 4	0	HXB2	>100		>100
9	279.3	2.98	44 ± 2	0	HXB2	141 ± 59		>100
10	514.6	7.84	1.4 ± 0.3	0	HXB2	3 ± 1		80
				2	Ba-L		14.6	>100
				5			49.6	>100
				10			92.1	>100
				10	IIIB		>100	>100
11	323.3	1.86	393 ± 31	0	HXB2	>400		>100

[a] The error given is the standard deviation of four measurements. [b] The error range given is the standard error of 2−5 measurements.

additional hydrophobic interactions with the surrounding pocket (**3b**,**c**) or (2) polar functionality (**3d**−**f**), including the possibility of accessing the Leu568′.O or Val570.O carbonyl group for an additional hydrogen bond (**3d**−**e**) (Figure 4A,C). However, all of the substitutions decreased binding affinity to varying extents as compared to **3a** (Figure 2) and led to lower biological activity as well (Table 1).

Modification by Addition of a Third or Fourth Ring System. The addition of a third and fourth heterocyclic or aromatic ring was investigated for its potential to generate higher hydrophobic content and an extended interaction surface typical of protein−protein interaction inhibitors. The data in Tables 1 and 2 indicate that this strategy was successful, resulting in significant improvement in binding affinity in some cases. A dimeric form of **3a**, compound **10**, showed improved activity.[23] Compound **6a** contained an aryl group attached at the indole nitrogen. It had higher binding and antifusion activity than **3a**. Compound **8a**, which contained a methoxybenzyl group attached at the indole nitrogen, did not have improved activity over **3a**. Compound **14c**, an isomer of **6a**, had similar binding affinity but slightly lower biological activity. Because of ready extension of the scaffold on both ends to match the shape of the groove, several variants based on **14c** were prepared. Compound **14d**, in which the *m*-methoxy group was replaced by a hydroxyl group, had slightly lower activity, suggesting that a hydrophobic moiety at the phenyl *m*-position may be preferred. Compound **14f** was designed to increase the hydrophobicity and occupy more space inside the hydrophobic pocket, by replacing the phenyl ring of **14c** with a 6-chloroquinoline. Compound **14i** was made as the 5-substituted isomer of **14f**. Improved binding was seen for **14i** and greater than 2-fold improved inhibition of viral replication. Compound **14f**, however, showed both weaker binding and reduced biological activity as compared to **14c**. A difference in activity between isomers was also observed for **3a** and **3g**, although in that case, the 6-substituted indole **3a** was more active (Table 1).[21] This difference indicated that a very specific interaction was occurring between the ligands and the residues in the pocket. Compounds **14b** and **14e** contained an additional one or two benzyloxy groups to make four or five ring systems, respectively, and both of these showed higher binding affinity. These two compounds have a large number of torsional degrees of freedom (10 and 13, respectively), which likely results in an entropic penalty upon binding. Inspired by the improved activity, we designed **14g** and **14h**, with the potential for shape complementarity to **14e** but with substantially reduced flexibility (8 torsional degrees of freedom). Compound **14g** demonstrated submicromolar binding, antifusion, and antiviral activity. Compound **14h** was also active in the sub- to low micromolar range. Compound **14g** and **14h** showed increased toxicity in 0% serum as compared to earlier compounds in the series, although their antifusion activity could clearly be discerned (Figure S2 in the Supporting Information), and serum had the effect of protecting the cells without substantially reducing the activity of the compounds.

Correlation between Binding Activity and Fusion Inhibitory Activity. A strong correlation was obtained between the hydrophobic pocket binding affinity (K_I) and the CCF EC_{50}, with R^2 = 0.91 (Figure 3 and Tables 1 and 2). This result suggested that inhibition of CCF was attributable to binding inside the hydrophobic pocket. This validates the use of the hydrophobic pocket as a target and verifies that the compounds are fusion inhibitors. The data indicated a 3−4-fold reduction in biological activity as compared to binding affinity and suggested an upper limit of ∼5 μM K_I to get substantial biological activity.

Correlation between Fusion Inhibitory Activity and Inhibition of Viral Replication. A very good agreement between fusion inhibition and inhibition of viral replication was observed for the indole compounds, barring the effect of serum concentration. Binding to serum is significant for many of the compounds, due to the propensity for serum albumin to bind to small lipophilic anionic compounds.[28,29] While this can improve ADME properties, it can also reduce the apparent efficacy of inhibitors that have micromolar activity, including many of the compounds described here. A clear and steady decrease in activity occurred with increased serum concentration in the assay (Tables 1 and 2). Fortunately, the effect of serum binding was mitigated for inhibitors with higher affinity for their intended target, observed here for **14g** and **14h**. The equilibrium appears to be shifted in favor of pocket binding for these inhibitors. It is significant that these molecules have equivalent inhibitory activity in binding, fusion, and viral replication, suggesting a clear mechanism of action with no off-target effects.

Analysis of Observed Binding Activity by Computational Docking. In the absence of experimental structural information on almost all of the compounds, we have analyzed compound activity by using the experimentally verified orientation of bound **3g**[21] and by looking for common binding modes that explained

Table 2. Molecular Weight, Inhibition Constants, Fusion and Viral Inhibitory Activity, and Cytotoxicity of Indole Compounds in Series 14 and 15

compd	mol. wt.	cLog *P*	obs. K_I (μM)[a]	% serum	virus strain	EC_{50} (μM) CCF [b]	EC_{50} (μM) HIV-1 replication	CC_{50} (μM) cytotoxicity [b]
14b	477.5	5.44	1.0 ± 0.2	0	HXB2	9 ± 2		>500
				2	Ba-L		34.2	>100
				5			56.2	>100
				10			>100	>100
				10	IIIB		>100	>100
14c	357.4	4.55	2.6 ± 0.3	0	HXB2	8 ± 2		>500
				2	Ba-L		18	67.5
				5			36.6	>100
				10			47.4	>100
				10	IIIB		57.4	>100
14d	343.4	4.35	4.3 ± 1.0	0	HXB2	14 ± 3		>100
				2	Ba-L		27.6	>100
				5			58.5	>100
				10			82.7	>100
				10	IIIB		>100	>100
14e	597.7	7.15	1.1 ± 0.3	0	HXB2	1.5 ± 0.2		>100
				2	Ba-L		13.8	58.9
				5			18.7	>100
				10			22.6	>100
				10	IIIB		34.3	>100
14f	412.9	5.64	3.9 ± 0.6	0	HXB2	13 ± 3		47
				2	Ba-L		48.0	>100
				5			88.5	>100
				10			>100	>100
				10	IIIB		>100	>100
14g	486.6	6.02	0.8 ± 0.2	0	HXB2	0.8 ± 0.2		19 ± 3
				2	Ba-L		0.92	50.1
				5			2.01	>100
				10			2.38	>100
				10	IIIB		2.80	>100
14h	474.2	6.18	1.1 ± 0.2	0	HXB2	0.54 ± 0.2		17 ± 3
				2	Ba-L		1.56	52.2
				5			3.30	98.5
				10			4.49	>100
				10	IIIB		5.20	>100
14i	412.9	5.64	1.5 ± 0.3	0	HXB2	8.3 ± 2		>100
				2	Ba-L		6.41	50.1
				5			10.1	>100
				10			13.1	>100
				10	IIIB		15.5	>100
15	237.3	3.25	14 ± 0.9			79 ± 15		>100

[a] The error given is the standard deviation of four measurements. [b] The error range given is the standard error of 2−5 measurements.

the observed structure−activity relationships. We docked the ligands into two receptor structures used in the NMR study, namely, 3p7k, an apo-gp41 structure (NHR, 2.3 Å resolution), and 2R5D, a bound D-peptide structure (IQN17/PIE7, 1.6 Å

resolution).[5] A single dihedral angle rotation on Lys574 Cδ-Cε was applied to 2r5d to rotate the side chain amine toward the pocket and make it accessible to small molecules binding in the pocket. This modification is in line with previous studies that showed the importance of the lysine in pocket interactions with both linear peptides[30] and small molecules.[15]

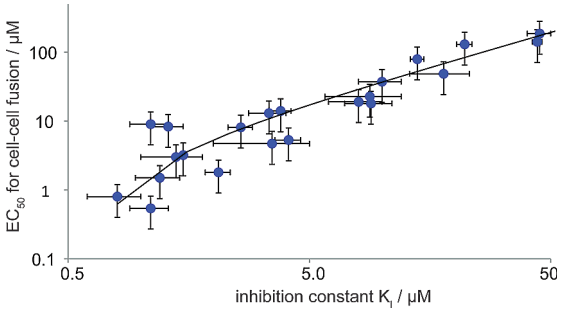

Figure 3. Comparison of observed inhibition constant for hydrophobic pocket binding with observed EC_{50} for inhibition of CCF. The data were obtained from Table 1, excluding inhibitors with EC_{50} > 100 μM. A log−log plot is presented, and a linear fit to the data is shown ($y = 3.92x - 2.51$; $R^2 = 0.915$).

Most of the compounds were observed to dock in one of two common binding modes with low energy and large cluster size. Examples of the poses are shown in Figure 4A,B (receptor 3p7k) and Figure S3 in the Supporting Information (receptor 2r5d). Very similar binding modes were obtained in both receptors. Compounds with two ring systems (**3a**−**g**) clustered tightly in pose 4A. They conformed to the expected orientation inferred from the position of **3g** determined by NMR experiments. The carboxylate group of **3g** formed an electrostatic interaction with Lys574, and the indole NH pointed toward the pocket.[21] On the basis of this structure, we reasoned that the 6-substituted isomer **3a** would dock similarly, with the NH pointing away from the pocket. This pose was found universally for **3a**−**f** with 3p7k and 2r5d. Hydrogen bonds were predicted between **3e** (*p*-OH) and the carbonyl oxygen of Leu568′ in 3p7k and between **3d** (*m*-OH) and the carbonyl oxygen of Val570 in 2r5d. In reality, **3d** and **3e** have weaker activity than **3a**, suggesting that these hydrogen

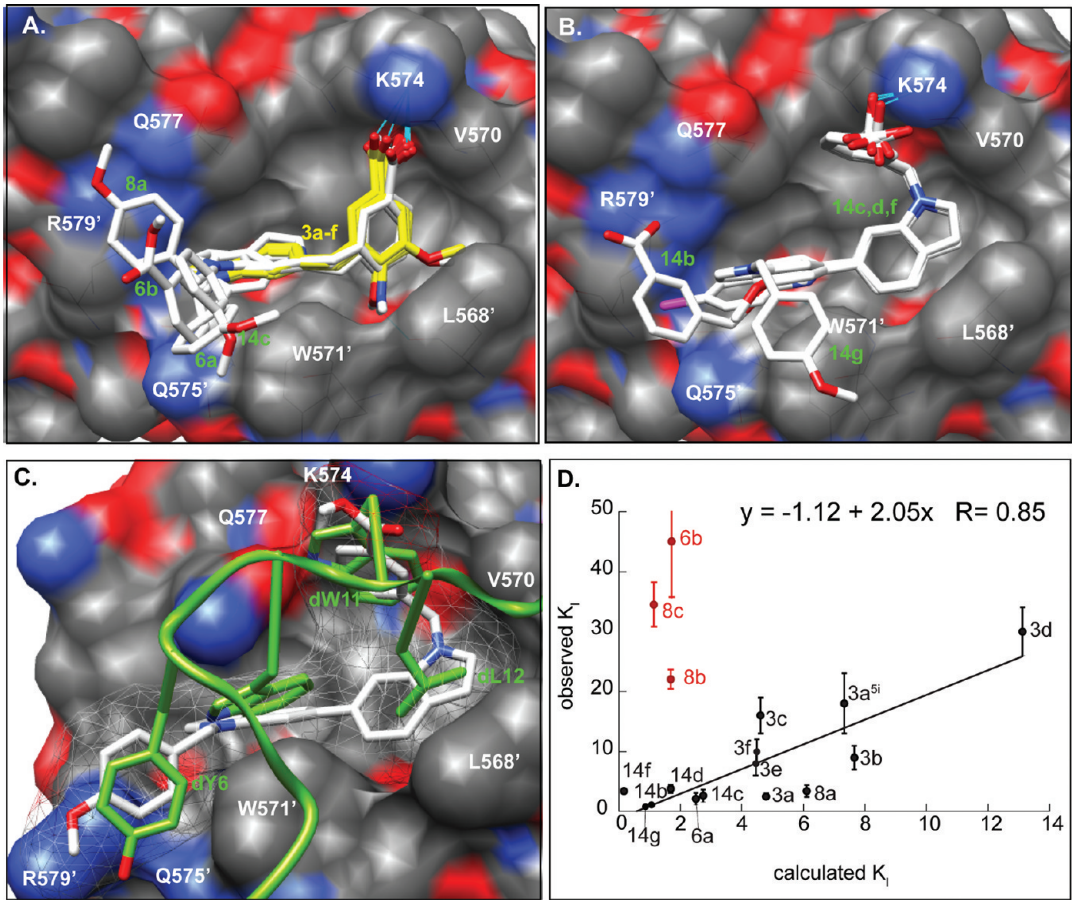

Figure 4. Predicted low energy, large cluster size poses in the hydrophobic pocket from Autodock4.2 simulations. (A) Receptor 3p7k, compounds in series **3** (in yellow), **6**, **8**, and **14c** (in white), specifically **3a** (1, 46%), **3b** (1, 78%), **3c** (1, 100%), **3d** (2, 61%), **3e** (1, 100%), **3f** (1, 98%), **6a** (1, 19%), **6b** (2, 27%), **8a** (2, 10%), and **14c** (1, 9%). (B) Receptor 3p7k, compounds in series **14** (Table 2), specifically **14b** (3, 10.5%), **14c** (2, 23%), **14d** (2, 19%), **14f** (1, 81%), and **14g** (1, 51%). The numbers in brackets indicate rank and cluster size as a percentage of all poses. Example hydrogen bonds to K574 are shown as blue lines. (C) Overlap of a low energy pose of **14g** (in white with a mesh surface) calculated by AutoDock4.2, with the experimental structure of the D-peptide PIE7 (in green) in the hydrophobic pocket of 2r5d. Only hydrophobic residues of PIE7 that interact in the pocket are shown explicitly. (D) Observed vs calculated inhibition constants in 3p7k. K_I were obtained from the calculated ΔG_{bind} according to the equation $K_I = \exp(\Delta G_{bind}/RT)$ at $T = 25$ °C, where $R = 1.987$ cal/K^{-1} mol^{-1}. A linear plot through the data is shown, together with the correlation coefficient R. Compounds shown in red were not included in the fit (see the text).

dx.doi.org/10.1021/jm200791z |J. Med. Chem. 2011, 54, 7220–7231

bonds do not form or do not contribute substantially to the binding energy.

Compounds with three ring systems including series **6** and **8** as well as compounds **14c** and **14d** could also dock in the pose shown in Figure 4A. However, an alternative low energy conformation of series **14** compounds (Table 2) was found in both 3p7k and 2r5d (Figure 4B and Figure S3B in the Supporting Information) that extended to four and five ring compounds. In this conformation, strong hydrophobic and electrostatic interactions occurred between the benzylcarboxylate and the pocket lysine, and the compounds curved around the pocket. Interestingly, these putative poses of the extended indole ligands followed the same S-shaped contour that is formed by the hydrophobic residues dY6, dW9, dW11, and dL12 of PIE7 in the pocket of 2r5d.[31] The overlap is shown for a predicted pose of the longest and one of the most potent indole compounds **14g** in Figure 4C. The indole rings occupied the same part of the pocket as dW9 and dL12, the carboxybenzyl group made similar hydrophobic contacts as dW11, and the methoxybenzyl group occupied the same channel as dY.

We observed tight clustering at the N-terminal end of the pocket and a larger variation in the adopted poses of ligand moieties at the C-terminal end. This correlated with a greater degree of variation in pocket side chains at the C-terminal end in different structures and lower hydrophobic contact with the ligands. It is clear that residue flexibility around the hydrophobic pocket required the inhibitors to adjust to the groove shape. Reciprocal compatibility between inhibitor and side chain flexibility is an important property of gp41 pocket inhibitors.

The orientation in Figure 4A explained the poor activity of compounds **9** and **11**, which have a polar substituent at position 3 of the indole ring. This position points toward the pocket, and polar substitution would be likely to destabilize the complex. An orientational rearrangement may occur. However, we did find for these molecules, as well as for molecules with three aromatic moieties and having polar groups at opposite ends (**6b**, **8b**, and **8c**), that docking predicted a much higher affinity than that observed, which is likely due to the fact that flexibility of Gln and Arg residues at the C-terminal edge of the pocket reduced the contribution of electrostatic interactions calculated for a rigid model.

In Figure 4D, a linear fit of calculated vs observed binding affinities is shown, excluding molecules that have polar groups at both ends (shown in red). A good correlation was observed, with a correlation coefficient $R = 0.85$. Calculated energies were not able to distinguish between the poses shown in Figure 4A,B for **14c** and **14d**.

CONCLUSION

In this study, we have designed, synthesized, and tested a series of indole compounds as inhibitors against gp41-mediated HIV-1 fusion. We have observed a strong correlation between hydrophobic pocket binding affinity and CCF fusion inhibition in the submicromolar to hundreds of micromolar range. The CCF results correlate well with the ability of the compounds to inhibit viral replication. This implies that the hydrophobic pocket is the target of these molecules. The set of compounds has enabled us to establish a direction for optimization. Specifically, we observed that elongating the compound caused significant improvement. Adding defined flexibility so that the compound could conform to the grooves of the coiled coil improved its activity. In general, adding polar groups at both ends reduced activity.

Computational docking suggested common binding modes for groups of inhibitors, and AutoDock4.2 calculations gave a good correlation with the observed relative rank order. Two- and three-ring compounds with polar groups at both ends were an exception, since they were predicted to have high affinity, but they actually were poor binders and fusion inhibitors.

Compounds **14g** and **14h** with a long hydrophobic interface showed submicromolar binding and fusion inhibition, and **14g** also had submicromolar inhibition of viral replication. To our knowledge, this is the best activity yet reported for a verified low molecular weight fusion inhibitor. A putative binding mode mimics the hydrophobic interactions of the D-peptide inhibitor PIE7. The binding models of **14g** and other indole compounds in Figure 4 explained the observation that addition of hydrophobic groups while maintaining shape complementarity was required to improve activity. It appears to be a more general property that amphiphilic structures, with separated polar and nonpolar ends, provide better inhibition of the gp41 hydrophobic pocket.[32] We will conduct lead optimization on this basis. Compounds with improved activity have elevated cLog *P* values and should be modified to increase solubility and reduce toxicity in consideration of absorption, distribution, metabolism, and excretion—toxicity in pharmacokinetics (ADMET) issues.[29,33] In addition, improved binding affinity to the hydrophobic pocket must be accompanied by reduced serum binding propensity.[29,34]

EXPERIMENTAL SECTION

Chemical reagents and solvents were used as received. HPLC was performed on a Waters Breeze HPLC with multi λ fluorescence detector and dual λ UV detector, using a water/acetonitrile or water/methanol gradient with 0.05% TFA. Mass spectra were determined by LCMS (Waters micromass ZQ: H_2O/acetonitrile gradient, with 0.1% formic acid). ^1H NMR spectra were determined at 400 MHz in dimethylsulfoxide (DMSO)-d_6, unless otherwise stated, using TMS as a reference.

Synthetic Procedures. The organic synthesis was carried out according to Schemes 1−3. Reaction conditions i−vii are described below. The main scaffold of the compounds (**2a**−**f** and **13a**−**g**) was synthesized by Suzuki coupling.[35] The Ullmann reaction was employed to add the phenyl ring at the 1 (NH) position of the indole ring.[36] Benzyl bromide intermediates for Suzuki coupling were synthesized by radical substitution using *N*-bromosuccinimide.[37] All compounds were purified by preparative HPLC, which resulted in ≥95% purity for assay testing.

*i: Suzuki Coupling—Synthesis of Methyl 3-(1H-Indol-6-ylmethyl) Benzoate (**2a**).* Indole-6-boronic acid (386 mg, 2.4 mmol) and methyl-3-(bromomethyl) benzoate (460 mg, 2.0 mmol) were added into a 100 mL round-bottomed flask containing tetrahydrofuran (THF) (15 mL); then, 115 mg of $Pd(PPh_3)_4$ was added, followed by 3 mL of 2 M K_2CO_3. The mixture was stirred and heated to reflux under N_2 for 4 h. The reaction was monitored by TLC. After the reaction was complete, the mixture was cooled to room temperature, 10 mL of H_2O was added, and the product was extracted with ethyl acetate (10 mL × 3). The organic solvent was combined, dried (anhydrous Na_2SO_4), filtered, and evaporated. The crude product was purified by chromatographic column using hexane:ethyl acetate (7:1) as eluent. A 360 mg amount of methyl 3-(1*H*-indol-6-ylmethyl) benzoate (**2a**) was obtained as pale yellow solid; yield, 67%. MS calcd for $C_{17}H_{15}NO_2$, 265. LC-MS: 266.01 $(M + H)^+$. ^1H NMR δ 10.99 (s, <1H, exch), 7.83 (s, 1H), 7.78 (d, J = 7.3 Hz, 1H), 7.55 (d, J = 7.3 Hz, 1H), 7.45 (s, 1H), 7.43 (s, 1H), 7.28 (t, J = 3.0 Hz, 1H), 7.22 (s, 1H), 6.87 (dd, J = 7.9, 1.2 Hz, 1H), 6.36 (s, 1H), 4.10 (s, 2H), 3.82 (s, 3H).

*ii: Ester Acidification—Synthesis of 3-(1H-Indol-6-ylmethyl)benzoic Acid (**3a**).* Twenty milligrams of **2a** was dissolved into 4 mL of THF: methanol (4:1), and 1 mL of 25% NaOH in H_2O was added. The mixture was stirred for 3 h at room temperature and then adjusted to pH 3.0 using 2 M HCl. The solution was extracted with CH_2Cl_2 (15 mL × 3). The organic solvent was combined and dried and then evaporated. The final product was purified by HPLC using an acetonitrile/H_2O gradient. After lyophilization, 11.2 mg of target compound was obtained as a gray powder; yield, 60%. 3-(1*H*-Indol-6-ylmethyl)benzoic acid (**3a**): MS calcd for $C_{16}H_{13}NO_2$, 251. LC-MS: 252.6 $(M + H)^+$. ^1H NMR: δ 10.97 (s, < 1H, exch), 7.78 (s, 1H), 7.74 (d, J = 7.8 Hz, 1H), 7.50 (d, J = 7.3 Hz, 1H), 7.38 (m, 2H), 7.29 (m, 2H), 6.95 (d, J = 8.5 Hz, 1H), 6.35 (s, 1H), 4.05 (s, 2H).

*3-(1H-Indol-6-ylmethyl)-5-methoxy-benzoic Acid (**3b**).* MS calcd for $C_{17}H_{15}NO_3$, 281. LC-MS: 282.6 $(M + H)^+$. ^1H NMR: δ 10.98 (s, <1H, exch), 7.44 (d, J = 8.5 Hz, 1H), 7.39 (s, 1H), 7.26 (m, 2H), 7.21 (s, 1H), 7.09 (t, J = 1.8 Hz, 1H), 6.88 (dd, J = 8.5, 1.2 Hz, 1H), 6.35 (s, 1H), 4.05 (s, 2H), 3.77 (s, 3H).

*4-(1H-Indol-6-ylmethyl)-5-methoxy-benzoic Acid (**3c**).* MS calcd for $C_{17}H_{15}NO_3$, 281. LC-MS: 282.8 $(M + H)^+$. ^1H NMR: δ 10.93 (s, <1H, exch), 7.80 (m, 1H), 7.65 (s, 1H), 7.42 (m, 1H), 7.25 (s, 1H), 7.17 (s, 1H), 7.08 (d, J = 7.3 Hz, 1H), 6.87 (m, 1H), 6.35 (s, 1H), 4.00 (s, 2H), 3.88 (s, 3H).

*3-Hydroxy-5-(1H-indol-6-ylmethyl)benzoic Acid (**3d**).* MS calcd for $C_{16}H_{13}NO_3$, 267. LC-MS: 268.6 $(M + H)^+$. ^1H NMR: δ 10.97 (s, <1H exch), 9.63 (s, <1H, exch), 7.44 (d, J = 7.9 Hz, 1H), 7.26 (m, 2H), 7.19 (s, 1H), 7.13 (d, J = 1.8 Hz, 1H), 6.85 (m, 2H), 6.35 (t, J = 1.8 Hz, 1H), 3.98 (s, 2H).

*4-Hydroxy-3-(1H-indol-6-ylmethyl)benzoic Acid (**3e**).* MS calcd for $C_{16}H_{13}NO_3$, 267. LC-MS: 268.5 $(M + H)^+$. ^1H NMR: δ 10.85 (s, < 1H, exch), 10.36 (s, < 1H, exch), 7.58 (m, 2H), 7.41 (d, J = 7.9 Hz, 1H), 7.32 (d, J = 7.9 Hz, 1H), 7.13 (d, J = 1.8 Hz, 1H), 7.03 (t, J = 7.9 Hz, 1H), 6.90 (m, 2H), 3.96 (s, 2H).

*3-(1H-Indol-6-ylmethyl)-4-nitro-benzoic Acid (**3f**).* MS calcd for $C_{16}H_{12}N_2O_4$, 296.3. LC-MS: 297.8 $(M + H)^+$. ^1H NMR: δ 11.00 (s, < 1H, exch), 7.98 (m, 3H), 7.45 (d, J = 7.9 Hz, 1H), 7.29 (t, J = 3.0 Hz, 1H), 7.13 (s, 1H), 6.80 (dd, J = 7.9, 1.2 Hz, 1H), 6.36 (s, 1H), 4.34 (s, 2H).

*3-((1H-Indol-5-yl)methyl)benzoic Acid (**3g**).* MS calcd for $C_{16}H_{13}NO_2$, 251. LC-MS: 252.6 $(M + H)^+$. ^1H NMR: δ 11.00 (s, <1H, exch), 7.78 (s, 1H), 7.74 (d, J = 7.9 Hz, 1H), 7.51 (d, J = 7.3 Hz, 1H), 7.38 (m, 2H), 7.29 (m, 2H), 6.95 (dd, J = 8.5, 1.2 Hz, 1H), 6.35 (s, 1H), 4.05 (s, 2H).

*iii: Ullman Reaction—Synthesis of 3-((1-(3-Methoxyphenyl)-1H-indol-6-yl)methyl)benzoic Acid (**6a**).* Twenty milligrams of **2a** was dissolved into 4 mL of DMSO, and 18 mg of 3-iodoanisole, 12 mg of potassium hydroxide, and 5 mg of Cu_2O catalyst were added. The mixture was stirred for 24 h at 135 °C under N_2. After it was cooled to room temperature, the mixture was treated as in general procedure ii. The final product was purified by HPLC using acetonitrile/H_2O as an eluent. After lyophilization, 3.5 mg of the target compound was obtained as a gray powder; yield, 13%. MS calcd for $C_{23}H_{19}NO_3$, 357. LC-MS: 358.7 $(M + H)^+$. ^1H NMR: δ 7.81 (s, 1H), 7.74 (d, J = 6.8 Hz, 1H), 7.61 (d, J = 3.0 Hz, 1H), 7.58 (d, J = 7.8 Hz, 1H), 7.49 (m, 3H), 7.39 (t, J = 6.8 Hz, 1H), 7.14 (d, J = 7.8 Hz, 1H), 7.08 (s, 1H), 7.01 (d, J = 7.8 Hz, 1H), 6.96 (d, J = 7.8 Hz, 1H), 6.64 (d, J = 2.4 Hz, 1H), 4.12 (s, 2H), 3.82 (s, 3H).

*3-(6-(3-Carboxybenzyl)-1H-indol-1-yl)benzoic Acid (**6b**).* MS calcd for $C_{23}H_{17}NO_4$, 371. LC-MS: 372.6 $(M + H)^+$. ^1H NMR: δ 8.02 (s, 1H), 7.95 (br, 2H), 7.86 (d, J = 8.8 Hz, 1H), 7.78 (s, 1H), 7.67 (m, 1H). 7.59 (d, J = 7.8 Hz, 1H), 7.49 (br, 2H), 7.39 (d, J = 7.8 Hz, 1H), 6.68 (br, 2H), 6.56 (s, 1H), 4.11(s, 2H).

*iv: Synthesis of 3-((1-(4-Methoxybenzyl)-1H-indol-6-yl)methyl)-benzoic Acid (**8a**).* Thirty-two milligrams of **2a** was dissolved into 4 mL of anhydrous DMF, and 15 mg of sodium hydride in oil (60%) was added. The mixture was cooled in an ice−water bath and stirred for 1 h at room temperature. Thirty-five milligrams of 4-methoxybenzylbromide was added, and the mixture was stirred at room temperature overnight. TLC indicated no starting material remained, and the reaction was quenched by adding 10 mL of water. The solution was extracted with ethyl acetate (15 mL × 3) or dichloromethane (15 mL × 3). The organic solvent was combined and evaporated, and the product directly was used for the next step without further purification. The ester group was saponified, following the general procedure ii to yield the target compound; crude yield, 95%. A 5.0 mg amount of purified target compound was obtained by HPLC as an off-white powder. MS calcd for $C_{24}H_{21}NO_3$, 371. LC-MS: 372 $(M + H)^+$. ^1H NMR: δ 7.77 (s, 1H), 7.72 (d, J = 7.7 Hz, 1H), 7.49 (d, J = 7.0 Hz, 1H), 7.43 (d, J = 2.5 Hz, 1H), 7.34 (br, 3H), 7.14 (d, J = 8.3 Hz, 2H), 6.95 (d, J = 7.7 Hz, 1H), 6.82 (d, J = 8.3 Hz, 2H), 6.37 (d, J = 2.6 Hz, 1H), 5.27 (s, 2H), 4.04 (s, 2H), 3.67 (s, 3H).

*3-((1-(3-(Carboxy)benzyl)-1H-indol-6-yl)methyl)benzoic Acid (**8b**).* MS calcd for $C_{24}H_{14}NO_4$, 385. LC-MS: 386.5 $(M + H)^+$. ^1H NMR: δ 7.78 (s, 1H), 7.72 (br, 2H), 7.68 (m, 1H), 7.60 (d, J = 7.9 Hz, 1H), 7.45 (d, J = 3.0 Hz, 1H), 7.34 (m, 3H), 7.30 (br, 2H), 7.08 (d, J = 7.9 Hz, 1H), 6.57 (d, J = 2.6 Hz, 1H), 5.42 (s, 2H), 4.09 (s, 2H).

*3-((1-(3-Carboxybenzyl)-1H-indol-5-yl)methyl)benzoic Acid (**8c**).* MS calcd for $C_{24}H_{14}NO_4$, 385. LC-MS: 386.7 $(M + H)^+$. ^1H NMR: δ 7.78 (d, J = 7.9 Hz, 3H), 7.73 (d, J = 7.9 Hz, 1H), 7.49 (br, 2H), 7.40 (br, 4H), 7.35 (d, J = 8.5 Hz, 1H), 6.97 (d, J = 8.5 Hz, 1H), 6.43 (d, J = 3.0 Hz, 1H), 5.46 (s, 2H), 4.04 (s, 2H).

*v: Synthesis of 3-((3-Formyl-1H-indol-6-yl)methyl)benzoic Acid (**9**).* Three milliliters of anhydrous DMF was cooled in an ice−water bath, then 50 μL of $POCl_3$ was added, the solution was stirred for about 15 min, and then 32 mg of **2a** in 2 mL of DMF was added. The mixture was heated to 40 °C for 3 h. After it was cooled to room temperature, the mixture was treated by cold water, following the general procedure ii; 11.2 mg of target compound was purified as a brown solid; yield, 34%. MS calcd for $C_{17}H_{13}NO_3$, 279. LC-MS: 280.6 $(M + H)^+$. ^1H NMR: δ 9.89 (s, 1H), 8.24 (d, J = 3.0 Hz, 1H), 7.98 (d, J = 7.3 Hz, 1H), 7.80 (s, 1H), 7.76 (d, J = 7.9 Hz, 1H), 7.52 (d, J = 7.9 Hz, 1H), 7.41 (t, J = 7.9 Hz, 1H), 7.34 (s, 1H), 7.12 (d, J = 7.3 Hz, 1H), 4.13 (s, 2H).

*vi: Synthesis of 3,3′-(1,1′-Methylenebis(1H-indole-6,1-diyl))bis-(methylene)dibenzoic Acid (**10**).* Thirty-two milligrams of **2a** was dissolved in 3 mL of DMSO, and then, 56 mg of KOH was added; the mixture was stirred at room temperature overnight under N_2. Then, 50 μL of CH_2Cl_2 was added, and the mixture was stirred for 8 h at room temperature. Then, following the general procedure ii, 3.6 mg of target compound was purified as an orange powder; yield, 12%. MS calcd for $C_{33}H_{26}N_2O_4$, 514. LC-MS: 515.1 $(M + H)^+$. ^1H NMR: δ 7.84 (s, 2H), 7.79 (s, 2H), 7.74 (d, J = 7.7 Hz, 2H), 7.62 (d, J = 3.2 Hz, 2H), 7.48 (d, J = 7.7 Hz, 2H), 7.39 (d, J = 1.9 Hz, 2H), 7.37 (d, J = 1.9 Hz, 2H), 6.90 (d, J = 8.3 Hz, 2H), 6.57 (s, 2H), 6.35 (d, J = 2.6 Hz, 2H), 4.07 (s, 4H).

*vii: Synthesis of 3-((3-(Carboxycarbonyl)-1H-indol-6-yl)methyl)-benzoic Acid (**11**).* Thirty-two milligrams of **2a** was treated by 2 M oxalyl dichloride in methylene chloride for 4 h at room temperature. Then, following the general procedure ii, part of the product was purified to yield 3.4 mg of target compound as a yellow powder; yield, 9%. MS calcd for $C_{18}H_{13}NO_5$, 323. LC-MS: 324.6 $(M + H)^+$. ^1H NMR: δ 11.52 (s,<1H, exch), 8.36 (d, J = 3.0 Hz, 1H), 8.07 (d, J = 7.9 Hz, 1H), 7.80 (s, 1H), 7.77 (d, J = 7.9 Hz, 1H), 7.54 (d, J = 7.9 Hz, 1H), 7.44 (br, 1H), 7.40 (s, 1H), 7.17 (d, J = 7.9 Hz, 1H), 4.13 (s, 2H).

*Synthesis of 2,6-Dichloro Quinoline (**12f**).* A 180 mg amount of 6-chloro-2-hydroxy quinoline was treated with 3 mL of $POCl_3$, and the mixture was refluxed for 3 h; the remaining $POCl_3$ was evaporated away. After it was cooled to room temperature, the residue was treated with cold water; the solid was filtered and dried, giving a green powder; yield, 90%. MS calcd for $C_9H_5Cl_2N$, 198. LC-MS: 200.1 $(M + 2)^+$. ^1H NMR in

$CDCl_3$: δ 8.04 (d, J = 7.8 Hz, 1H), 7.97 (d, J = 8.8 Hz, 1H), 7.81 (d, J = 1.9 Hz, 1H), 7.69 (dd, J = 9.8, 2.9 Hz, 1H), 7.42 (d, J = 8.8 Hz, 1H).

*1-(4-Methoxyphenyl)methyl-6-bromoindole (**12g**).* ^{1}H NMR: δ 7.73 (s, 1H), 7.51 (br, 2H), 7.17 (d, J = 8.5 Hz, 2H), 7.12 (dd, J = 8.5, 1.2 Hz, 1H), 6.87 (d, J = 8.5 Hz, 2H), 6.49 (d, J = 3.0 Hz, 1H), 5.34 (s, 2H), 3.70 (s, 3H).

*6-(3-Hydroxyphenyl)-1H-indole (**13b**).* MS calcd for $C_{14}H_{11}NO$, 209. LC-MS: 210.5 $(M + H)^+$. ^{1}H NMR: δ 9.46 (s, <1H, exch), 7.58 (m, 2H), 7.38 (t, J = 2.9 Hz, 1H), 7.23 (m, 2H), 7.07 (d, J = 7.8 Hz, 1H), 7.04 (d, J = 1.9 Hz, 1H), 6.71 (dd, J = 7.8, 1.9 Hz, 1H), 6.44 (s, 1H).

*6-(3-Methoxyphenyl)-1H-indole (**13c**).* MS calcd for $C_{15}H_{13}NO$, 223. LC-MS: 224.6 $(M + H)^+$. ^{1}H NMR: δ 11.16 (s, <1H, exch), 7.63 (s, 1H), 7.59 (d, J = 7.9 Hz, 1H), 7.37 (t, J = 3.0 Hz, 1H), 7.34 (d, J = 7.9 Hz, 1H), 7.30 (dd, J = 7.9, 1.8 Hz, 1H), 7.23 (d, J = 7.9 Hz, 1H), 7.17 (br, 1H), 6.89 (dd, J = 8.5, 1.8 Hz, 1H), 6.44 (s, 1H), 3.82 (s, 3H).

*6-[3-[(4-Methoxyphenyl)methoxy]phenyl]-1H-indole (**13e**).* ^{1}H NMR (400 MHz): δ 7.49 (s, 1H), 7.38 (s, 1H), 7.34 (s, 1H), 7.33 (d, J = 1.9 Hz, 1H), 7.28 (t, J = 7.8 Hz, 1H), 7.17 (d, J = 8.8 Hz, 1H), 7.11 (d, J = 2.9 Hz, 2H), 7.07 (d, J = 5.9 Hz, 1H), 6.96 (d, J = 9.8 Hz, 1H), 6.90 (d, J = 8.8 Hz, 2H), 6.87 (dd, J = 8.8, 1.9 Hz, 1H), 5.04 (s, 2H), 3.74 (s, 3H).

*6-(6-Chloro-2-quinolyl) Indole (**13f**).* MS calcd for $C_{11}H_{17}ClN_2$, 278. LC-MS: 280.8 $(M + 2)^+$. ^{1}H NMR in $CDCl_3$: δ 8.33 (s, 1H), 8.12 (t, J = 8.8 Hz, 2H), 7.99 (d, J = 8.8 Hz, 1H), 7.90 (dd, J = 7.8, 1.9 Hz, 1H), 7.81 (d, J = 1.9 Hz, 1H), 7.78 (d, J = 7.8 Hz, 1H), 7.65 (dd, J = 8.8, 1.9 Hz, 1H), 7.32 (t, J = 2.9 Hz, 1H), 6.62 (s, 1H).

*6-[1-[(4-Methoxyphenyl)methyl]indol-6-yl]-indole (**13g**).* MS calcd for $C_{24}H_{20}N_2O$, 352. LC-MS: 335.8 $(M + H - H_2O)^+$. ^{1}H NMR: δ 7.72 (s, 1H), 7.68 (m, 1H),7.62 (s, 1H), 7.61 (d, J = 3.6 Hz, 1H), 7.59 (d, J = 4.3 Hz, 1H), 7.48 (d, J = 3.0 Hz, 1H), 7.34 (s, 1H), 7.31 (d, J = 7.3 Hz, 1H), 7.21 (d, J = 8.5 Hz, 2H), 6.87 (d, J = 8.5 Hz, 2H), 6.47 (d, J = 3.0 Hz, 1H), 6.43 (s, 1H), 5.42 (s, 2H), 3.68 (s, 3H).

*5-(6-Chloro-2-quinolyl) Indole (**13i**).* MS calcd for $C_{11}H_{17}ClN_2$, 278. LC-MS: 279.1 $(M + H)^+$. ^{1}H NMR in $CDCl_3$: δ 8.45 (s, 1H), 8.11 (m, 3H), 7.99 (d, J = 8.8 Hz, 1H), 7.91 (dd, J = 11.0, 7.8 Hz, 1H), 7.80 (d, J = 1.9 Hz, 1H), 7.64 (dd, J = 8.8, 1.9 Hz, 1H), 7.54 (d, J = 8.8 Hz, 1H), 7.19 (t, J = 2.9 Hz, 1H), 6.69 (s, 1H).

*3-((3-(1-(3-Carboxybenzyl)-1H-indol-6-yl)phenoxy)methyl)benzoic Acid (**14b**).* MS calcd for $C_{30}H_{23}NO_5$, 477. LC-MS: 478.1 $(M + H)^+$. ^{1}H NMR: δ 8.07 (s, 1H), 7.91 (d, J = 7.8 Hz, 1H), 7.79 (m, 3H), 7.73 (d, J = 7.8 Hz, 1H), 7.62 (d, J = 7.8 Hz, 1H), 7.56 (d, J = 3.9 Hz, 1H), 7.53 (d, J = 7.8 Hz, 1H), 7.44 (m, 2H), 7.33 (m, 2H), 7.30 (d, J = 1.9 Hz, 1H), 7.25 (d, J = 7.8 Hz, 1H), 6.97 (dd, J = 8.8,1.9 Hz, 1H,), 6.53 (d, J = 2.9 Hz, 1H), 5.60 (s, 2H), 5.26 (s, 2H).

*3-((6-(3-Methoxyphenyl)-1H-indol-1-yl)methyl)benzoic Acid (Compound **14c**).* MS calcd for $C_{23}H_{19}NO_3$, 357. LC-MS: 358.7 $(M + H)^+$. ^{1}H NMR: δ 7.82 (s, 1H), 7.81 (s, 1H),7.77 (s, 1H), 7.62 (d, J = 8.5 Hz, 1H), 7.57 (d, J = 2.4 Hz, 1H), 7.46 (m, 2H), 7.34 (m, 2H), 7.23 (d, J = 7.3 Hz, 1H), 7.18 (s, 1H), 6.88 (dd, J = 7.9, 1.9 Hz, 1H), 6.53 (d, J = 2.9 Hz, 1H), 5.60 (s, 2H), 3.82 (s, 3H).

*3-((6-(3-Hydroxyphenyl)-1H-indol-1-yl)methyl)benzoic Acid (**14d**).* MS calcd for $C_{22}H_{17}NO_3$, 343. LC-MS: 344.1 $(M + H)^+$. ^{1}H NMR: δ 8.07 (s, 1H), 7.90 (d, J = 7.8 Hz, 1H), 7.74 (d, J = 6.8 Hz, 1H), 7.63 (s, 1H), 7.59 (d, J = 8.8 Hz 1H), 7.54 (t, J = 7.8 Hz, 1H), 7.36 (m, 2H), 7.29 (br, 2H), 7.25 (d, J = 7.8 Hz, 1H), 6.97 (d, J = 7.8 Hz, 1H), 6.44 (s, 1H), 5.28 (s, 2H).

*3-((3-((6-(3-(4-Methoxybenzyloxy)phenyl)-1H-indol-1-yl)methyl) benzoyloxy)methyl) benzoic Acid (**14e**).* MS calcd for $C_{39}H_{31}NO_6$, 597. LC-MS: 598.1 $(M + H)^+$. ^{1}H NMR: δ 8.02 (s, 1H), 7.89 (d, J = 7.8 Hz, 1H), 7.78 (d, J = 6.8 Hz, 1H), 7.75 (s, 1H), 7.68 (d, J = 7.8 Hz, 1H), 7.57 (br, 2H), 7.50 (t, J = 7.8 Hz, 1H), 7.37 (m, 2H), 7.31 (s, 1H), 7.07 (d, J = 8.8 Hz, 1H), 6.92 (m, 2H), 6.84 (d, J = 2.9 Hz, 1H), 6.69 (m, 5H), 6.54 (d, J = 2.9 Hz, 1H), 5.45 (s, 2H), 5.17 (s, 2H), 3.71 (s, 2H), 3.66 (s, 3H).

*3-[[6-(6-Chloro-2-quinolyl)indol-1-yl]methyl]benzoic Acid (**14f**).* MS calcd for $C_{25}H_{17}ClN_2O_2$, 412.8. LC-MS: 415.1 $(M + 2)^+$. ^{1}H NMR: δ 8.53 (s, 1H), 8.39 (d, J = 8.5 Hz, 1H), 8.24 (d, J = 8.5 Hz, 1H), 8.10 (dd, J = 8.5, 1.8 Hz, 2H), 8.05 (d, J = 9.2 Hz, 1H), 7.83 (dd, J = 6.7, 1.8 Hz, 1H), 7.79 (s, 1H), 7.75 (m, 1H), 7.62 (m, 2H), 7.45 (m, 2H), 6.68 (d, J = 3.0 Hz, 1H), 5.58 (s, 2H).

*3-[[6-[1-[(4-Methoxyphenyl)methyl]indol-6-yl]indol-1-yl]methyl]benzoic Acid (**14g**).* MS calcd for $C_{32}H_{26}N_2O_3$, 486. LC-MS: 487.8 $(M + H)^+$. ^{1}H NMR: δ 7.83 (br, 2H), 7.69 (d, J = 8.5 Hz, 2H), 7.60 (t, J = 8.5 Hz, 2H), 7.55 (t, J = 3.0 Hz, 2H), 7.46 (br, 2H), 7.35 (m, 2H), 7.20 (d, J = 8.5 Hz, 2H), 6.84 (d, J = 8.5 Hz, 2H), 6.51 (d, J = 3.0 Hz, 1H), 6.45 (d, J = 3.0 Hz, 1H), 5.60 (s, 2H), 5.39 (s, 2H), 3.66 (s, 3H).

*3-[[6-[1-[(4-Fluoro)methyl]indol-6-yl]indol-1-yl]methyl]benzoic Acid (**14h**).* MS calcd for $C_{31}H_{23}FN_2O_2$, 474.2. LC-MS: 473 $(M - H)^-$. ^{1}H NMR: δ 7.82 (br, 2H), 7.69 (d, J = 4.8 Hz, 2H), 7.60 (t, J = 8.8 Hz, 2H), 7.54 (d, J = 2.9 Hz, 1H), 7.51 (d, J = 2.9 Hz, 1H), 7.45 (m, 2H), 7.35 (m, 2H), 7.27 (dd, J = 6.8, 5.8 Hz, 2H), 7.12 (t, J = 8.8 Hz, 2H), 6.51 (d, J = 2.9 Hz, 1H), 6.48 (d, J = 2.9 Hz, 1H), 5.59 (s, 2H), 5.48 (s, 2H).

*3-[[5-(6-Chloro-2-quinolyl)indol-1-yl]methyl]benzoic Acid (**14i**).* MS calcd for $C_{25}H_{17}ClN_2O_2$, 413. LC-MS: 415.3 $(M + 2)^+$. ^{1}H NMR: δ 8.42 (s, 1H), 8.40 (d, J = 9.2 Hz, 1H), 8.27 (d, J = 8.5 Hz, 1H), 8.10 (d, J = 2.4 Hz, 1H), 8.04 (d, J = 8.5 Hz, 2H), 7.81 (br, 2H), 7.72 (m, 2H), 7.67 (d, J = 3.0 Hz, 1H), 7.48 (m, 2H), 6.59 (d, J = 2.4 Hz, 1H), 5.67 (s, 2H).

*3-(1H-Indol-6-yl)benzoic Acid (**15**).* MS calcd for $C_{15}H_{11}NO_2$, 237. LC-MS: 220.1 $(M + H - H_2O)^+$. ^{1}H NMR: δ 11.21 (s, 1H), 8.21 (s, 1H), 7.93 (d, J = 7.3 Hz, 1H), 7.89 (d, J = 7.3 Hz, 1H), 7.67 (s, 1H), 7.64 (d, J = 7.3 Hz, 1H), 7.58 (t, J = 7.9 Hz, 1H), 7.41 (br, 1H), 7.33 (d, J = 7.9 Hz, 1H), 6.47 (s, 1H).

Binding Affinity Assay. Inhibition constants K_I for binding in the hydrophobic pocket were determined using a fluorescence intensity assay as previously described.[23,24] Briefly, a metallopeptide receptor structure $Fe^{II}(env2.0)_3$ was used to mimic the hydrophobic pocket in the gp41 coiled coil. Env2.0 contains 17 hydrophobic pocket residues flanked by five residues on either side. Mixing $Fe^{II}(env2.0)_3$ with a fluorescein labeled pocket-binding C-peptide C18-FL caused quenching of fluorescence, which could be reversed in the presence of a competitive inhibitor. Typically, 7 μM binding sites (three per receptor trimer) and 7.5 nM C18-FL were used in the assay.

CCF Assay. CCF was measured following a published procedure[25] and using cell lines obtained through the NIH AIDS Research and Reference Reagent Program, Division of AIDS, NIAID, NIH. TZM-bl cells (#8129, contributed by J. C. Kappes, X. Wu, and Tranzyme Inc.) expressing CD4, CCR5, and CXCR4[38] and containing an integrated reporter gene for firefly luciferase under control of HIV-1 LTR[39] were used as target cells. They were grown overnight in 96 well plates in Dulbecco's modified Eagle medium (DMEM) supplemented with 10% fetal bovine serum (FBS), using 25000 cells per well. The following day, the medium was exchanged with reduced serum medium (Gibco), and 1 μL of compound in DMSO was added to each well, using 6−10 serial dilutions to obtain dose−response curves. HL2/3 effector cells (#1294, contributed by B. K. Felber and G. N. Pavlakis), which produce HXB2 Env, Tat, and Rev[40] were added, using 50000 cells per well, to a total well volume of 100 μL. After 6 h, luciferase expression was measured using Luciferase Assay Reagent (Promega). Controls containing 1 μL of DMSO with and without HL2/3 cells were measured for each compound, and experiments were performed in duplicate.

Viral Replication Assay. Inhibition of HIV-1 replication was determined in CCR5- and CXCR4-tropic MAGI antiviral assays as previously described.[26,27] HIV-1 isolates and cells were obtained from the NIH AIDS Research and Reference Reagent Program, Division of AIDS, NIAID, NIH, as follows: HIV-1 Ba-L from Suzanne Gartner, Mikulas Popovic, and Robert Gallo.[26,41] HIV-1 IIIB from Robert C. Gallo[26,42] MAGI-CCR5 cells from Dr. Julie Overbaugh.[43,44] Briefly,

MAGI-CCR5 cells were grown overnight in 96-well plates in DMEM supplemented with 10% FBS, using 10000 cells per well. The following day, the medium was removed, and compounds diluted in medium were added (six dilutions in triplicate at each dilution), followed by the addition of either HIV-1 Ba-L (CCR5-tropic assay) or HIV-1 IIIB (CXCR4-tropic assay) at approximately 10 50% tissue culture infective doses per well (~10 TCID50/well). Assay plates were incubated for 48 h, after which medium was removed and HIV-1 Tat-induced β-Gal enzyme expression was determined by chemiluminescence using Tropix Gal-Screen (Applied Biosystems) according to the manufacturer's instructions. For the evaluation of serum effects on compound efficacy, assays for HIV-1 Ba-L were conducted at serum concentrations of 2, 5, and 10%.

Cytotoxicity Assay. The cytotoxic effect of the compounds was determined using the identical cell culture procedure to that described above for fusion but measuring cell death using Cytotox Glo (Promega) instead of luciferase expression or using an Alamar Blue cell viability reagent (Invitrogen). Similarly, the cytotoxic effect of compounds evaluated in the viral replication assay was determined in uninfected MAGI-CCR5 cell cultures prepared and incubated identically to the infected cultures (virus inoculum replaced with media), with cell viability determined using 3-(4,5-dimethylthiazol-2-yl)-5-(3-carboxymethoxyphenyl)-2-(4-sulfophenyl)-2*H*-tetrazolium (MTS; CellTiter96 Reagent, Promega) following the manufacturer's protocol. For the evaluation of serum effects on compound cytotoxicity, assays in MAGI-CCR5 cells were conducted at serum concentrations of 2, 5, and 10%.

Computational Docking. The 3D coordinates of each ligand were generated from their SMILES strings using OMEGA2 and SZYBKI (OpenEye, Inc.). AutoDock4.2 (Scripps Research Institute) was used for docking, according to the procedure provided by the authors.[45] The default atom types and parameters supplied with AutoDock4.2 were used throughout this study. The grid dimensions were chosen to be between 15 and 26 Å in each dimension with 0.375 Å spacing between grid points, ensuring that the grid was large enough to cover the entire pocket and fine enough to sample the molecular characteristics of the pocket. One to two hundred docked conformations were calculated for each inhibitor and clustered according to default settings. Docking of the indole series was performed with two receptor structures, 2r5d and 3p7k, keeping each structure rigid during the docking process. In 2r5d, a dihedral angle change of −126° was applied to the Cδ−Cε bond of the Lys574, rotating the lysine side chain amine to be accessible to small molecules bound in the pocket.

■ ASSOCIATED CONTENT

Supporting Information. Figures showing the structure of 5-substituted indole compounds described in the text; examples of CCF, viral replication, and cytotoxicity dose−response curves for several compounds; and predicted docked structures of compounds in receptor 2r5d. This material is available free of charge via the Internet at http://pubs.acs.org.

■ AUTHOR INFORMATION

Corresponding Author

*Tel: 707-638-5492. Fax: 707-638-5255. E-mail: guangyan.zhou@tu.edu (G.Z.). Tel: 707-638-5463. Fax: 707-638-5255. E-mail: miriam.gochin@tu.edu (M.G.).

■ ACKNOWLEDGMENT

This work was supported by NIH Grants NS059403 and AI093243. Molecular graphics images were produced using the UCSF Chimera package from the Resource for Biocomputing, Visualization, and Informatics at the University of California, San Francisco (supported by NIH P41 RR-01081). We thank Dr. Eric Springman at Locus Pharmaceuticals (currently Ansaris) for providing the coordinates of 3p7k prior to publication. We thank M. Anderson for helpful suggestions on computational simulations and structure comparisons.

■ ABBREVIATIONS USED

CHR, C-terminal heptad repeat; NHR, N-terminal heptad repeat; CCF, cell−cell fusion; 6-HB, six-helix bundle; THF, tetrahydrofuran; DMSO, dimethylsulfoxide; FDA, Food and Drug Administration; DMEM, Dulbecco's modified Eagle medium; FBS, fetal bovine serum; EC_{50}, effective concentration for 50% inhibition; ADMET, absorption, distribution, metabolism, and excretion−toxicity in pharmacokinetics

■ REFERENCES

(1) Caffrey, M.; Cai, M.; Kaufman, J.; Stahl, S. J.; Wingfield, P. T.; Covell, D. G.; Gronenborn, A. M.; Clore, G. M. Three-dimensional solution structure of the 44 kDa ectodomain of SIV gp41. *EMBO J.* **1998**, *17*, 4572–4584.

(2) Chan, D. C.; Fass, D.; Berger, J. M.; Kim, P. S. Core structure of gp41 from the HIV envelope glycoprotein. *Cell* **1997**, *89*, 263–273.

(3) Gallo, S. A.; Puri, A.; Blumenthal, R. HIV-1 gp41 six-helix bundle formation occurs rapidly after the engagement of gp120 by CXCR4 in the HIV-1 Env-mediated fusion process. *Biochemistry (Moscow)* **2001**, *40*, 12231–12236.

(4) Matthews, T.; Salgo, M.; Greenberg, M.; Chung, J.; DeMasi, R.; Bolognesi, D. Enfuvirtide: The first therapy to inhibit the entry of HIV-1 into host CD4 lymphocytes. *Nat. Rev. Drug Discovery* **2004**, *3*, 215–225.

(5) Welch, B. D.; VanDemark, A. P.; Heroux, A.; Hill, C. P.; Kay, M. S. Potent D-peptide inhibitors of HIV-1 entry. *Proc. Natl. Acad. Sci. U.S.A.* **2007**, *104*, 16828–16833.

(6) Eckert, D. M.; Malashkevich, V. N.; Hong, L. H.; Carr, P. A.; Kim, P. S. Inhibiting HIV-1 entry: discovery of D-peptide inhibitors that target the gp41 coiled-coil pocket. *Cell* **1999**, *99*, 103–115.

(7) Welch, B. D.; Francis, J. N.; Redman, J. S.; Paul, S.; Weinstock, M. T.; Reeves, J. D.; Lie, Y. S.; Whitby, F. G.; Eckert, D. M.; Hill, C. P.; Root, M. J.; Kay, M. S. Design of a potent D-peptide HIV-1 entry inhibitor with a strong barrier to resistance. *J. Virol.* **2010**, *84*, 11235–11244.

(8) Chan, D. C.; Chutkowski, C. T.; Kim, P. S. Evidence that a prominent cavity in the coiled coil of HIV type 1 gp41 is an attractive drug target. *Proc. Natl. Acad. Sci. U.S.A.* **1998**, *95*, 15613–15617.

(9) Liu, S.; Wu, S.; Jiang, S. HIV entry inhibitors targeting gp41: From polypeptides to small-molecule compounds. *Curr. Pharm. Des.* **2007**, *13*, 143–162.

(10) Ernst, J. T.; Kutzki, O.; Debnath, A. K.; Jiang, S.; Lu, H.; Hamilton, A. D. Design of a protein surface antagonist based on alpha-helix mimicry: inhibition of gp41 assembly and viral fusion. *Angew. Chem., Int. Ed. Engl.* **2002**, *41*, 278–281.

(11) Jiang, S.; Lu, H.; Liu, S.; Zhao, Q.; He, Y.; Debnath, A. K. N-Substituted Pyrrole Derivatives as Novel Human Immunodeficiency Virus Type 1 Entry Inhibitors. *Antimicrob. Agents Chemother.* **2004**, *48*, 4349–4359.

(12) Teixeira, C.; Barbault, F.; Rebehmed, J.; Liu, K.; Xie, L.; Lu, H.; Jiang, S.; Fan, B.; Maurel, F. Molecular modeling studies of N-substituted pyrrole derivatives—Potential HIV-1 gp41 inhibitors. *Bioorg. Med. Chem.* **2008**, *16*, 3039–3048.

(13) Liu, K.; Lu, H.; Hou, L.; Qi, Z.; Teixeira, C.; Barbault, F.; Fan, B. T.; Liu, S.; Jiang, S.; Xie, L. Design, synthesis, and biological evaluation of N-carboxyphenylpyrrole derivatives as potent HIV fusion inhibitors targeting gp41. *J. Med. Chem.* **2008**, *51*, 7843–7854.

(14) Wang, Y.; Lu, H.; Zhu, Q.; Jiang, S.; Liao, Y. Structure-based design, synthesis and biological evaluation of new N-carboxyphenylpyrrole

derivatives as HIV fusion inhibitors targeting gp41. *Bioorg. Med. Chem. Lett.* **2010**, *20*, 189–192.

(15) Katritzky, A. R.; Tala, S. R.; Lu, H.; Vakulenko, A. V.; Chen, Q. Y.; Sivapackiam, J.; Pandya, K.; Jiang, S.; Debnath, A. K. Design, synthesis, and structure-activity relationship of a novel series of 2-aryl 5-(4-oxo-3-phenethyl-2-thioxothiazolidinylidenemethyl)furans as HIV-1 entry inhibitors. *J. Med. Chem.* **2009**, *52*, 7631–7639.

(16) Jiang, S.; Tala, S. R.; Lu, H.; Abo-Dya, N. E.; Avan, I.; Gyanda, K.; Lu, L.; Katritzky, A. R.; Debnath, A. K. Design, Synthesis, and Biological Activity of Novel 5-((Arylfuran/1H-pyrrol-2-yl)methylene)-2-thioxo-3-(3-(trifluoromethyl)phe nyl)thiazolidin-4-ones as HIV-1 Fusion Inhibitors Targeting gp41. *J. Med. Chem.* **2011**, *54*, 572–579.

(17) Frey, G.; Rits-Volloch, S.; Zhang, X. Q.; Schooley, R. T.; Chen, B.; Harrison, S. C. Small molecules that bind the inner core of gp41 and inhibit HIV envelope-mediated fusion. *Proc. Natl. Acad. Sci. U.S.A.* **2006**, *103*, 13938–13943.

(18) Xu, Y.; Lu, H.; Kennedy, J. P.; Yan, X.; McAllister, L. A.; Yamamoto, N.; Moss, J. A.; Boldt, G. E.; Jiang, S.; Janda, K. D. Evaluation of "credit card" libraries for inhibition of HIV-1 gp41 fusogenic core formation. *J. Comb. Chem.* **2006**, *8*, 531–539.

(19) Stewart, K. D.; Huth, J. R.; Ng, T. I.; McDaniel, K.; Hutchinson, R. N.; Stoll, V. S.; Mendoza, R. R.; Matayoshi, E. D.; Carrick, R.; Mo, H.; Severin, J.; Walter, K.; Richardson, P. L.; Barrett, L. W.; Meadows, R.; Anderson, S.; Kohlbrenner, W.; Maring, C.; Kempf, D. J.; Molla, A.; Olejniczak, E. T. Non-peptide entry inhibitors of HIV-1 that target the gp41 coiled coil pocket. *Bioorg. Med. Chem. Lett.* **2010**, *20*, 612–617.

(20) Balogh, E.; Wu, D.; Zhou, G.; Gochin, M. NMR Second Site Screening for Structure Determination of Ligands Bound in the Hydrophobic Pocket of HIV-1 gp41. *J. Am. Chem. Soc.* **2009**, *131*, 2821–2823.

(21) Gochin, M.; Zhou, G.; Phillips, A. H. Paramagnetic relaxation assisted docking of a small indole compound in the HIV-1 gp41 hydrophobic pocket. *ACS Chem. Biol.* **2010**, *6*, 267–274.

(22) Wells, J. A.; McClendon, C. L. Reaching for high-hanging fruit in drug discovery at protein-protein interfaces. *Nature* **2007**, *450*, 1001–1009.

(23) Zhou, G.; Wu, D.; Hermel, E.; Balogh, E.; Gochin, M. Design, synthesis, and evaluation of indole compounds as novel inhibitors targeting Gp41. *Bioorg. Med. Chem. Lett.* **2010**, *20*, 1500–1503.

(24) Cai, L.; Gochin, M. A Novel Fluorescence Intensity Screening Assay Identifies New Low Molecular Weight Inhibitors of the gp41 Coiled Coil Domain of HIV-1. *Antimicrob. Agents Chemother.* **2007**, *51*, 2388–2395.

(25) Wexler-Cohen, Y.; Shai, Y. Demonstrating the C-terminal boundary of the HIV 1 fusion conformation in a dynamic ongoing fusion process and implication for fusion inhibition. *FASEB J.* **2007**, *21*, 3677–3684.

(26) Kagiampakis, I.; Gharibi, A.; Mankowski, M. K.; Snyder, B. A.; Ptak, R. G.; Alatas, K.; LiWang, P. J. Potent strategy to inhibit HIV-1 by binding both gp120 and gp41. *Antimicrob. Agents Chemother.* **2011**, *55*, 264–275.

(27) Lackman-Smith, C.; Osterling, C.; Luckenbaugh, K.; Mankowski, M.; Snyder, B.; Lewis, G.; Paull, J.; Profy, A.; Ptak, R. G.; Buckheit, R. W., Jr.; Watson, K. M.; Cummins, J. E., Jr.; Sanders-Beer, B. E. Development of a comprehensive human immunodeficiency virus type 1 screening algorithm for discovery and preclinical testing of topical microbicides. *Antimicrob. Agents Chemother.* **2008**, *52*, 1768–1781.

(28) Curry, S. Lessons from the crystallographic analysis of small molecule binding to human serum albumin. *Drug Metab. Pharmacokinet.* **2009**, *24*, 342–357.

(29) Wendt, M. D. Discovery of ABT-263, a Bcl-family protein inhibitor: Observations on targeting a large protein−protein interaction. *Expert Opin. Drug Discovery* **2008**, *3*, 1123–1143.

(30) Jiang, S.; Debnath, A. K. A salt bridge between an N-terminal coiled coil of gp41 and an antiviral agent targeted to the gp41 core is important for anti-HIV-1 activity. *Biochem. Biophys. Res. Commun.* **2000**, *270*, 153–157.

(31) Welch, B. D.; VanDemark, A. P.; Heroux, A.; Hill, C. P.; Kay, M. S. Potent D-peptide inhibitors of HIV-1 entry. *Proc. Natl. Acad. Sci. U.S.A.* **2007**, *104*, 16828–16833.

(32) Gochin, M.; Zhou, G. Amphipathic properties of HIV-1 gp41 fusion inhibitors. *Curr. Top. Med. Chem.* **2011**in press.

(33) Lin, J.; Sahakian, D. C.; de Morais, S. M.; Xu, J. J.; Polzer, R. J.; Winter, S. M. The role of absorption, distribution, metabolism, excretion and toxicity in drug discovery. *Curr. Top. Med. Chem.* **2003**, *3*, 1125–1154.

(34) Hajduk, P. J.; Mendoza, R.; Petros, A. M.; Huth, J. R.; Bures, M.; Fesik, S. W.; Martin, Y. C. Ligand binding to domain-3 of human serum albumin: a chemometric analysis. *J. Comput.-Aided Mol. Des.* **2003**, *17*, 93–102.

(35) Miyaura, N.; Suzuki, A. Palladium-Catalyzed Cross-Coupling Reactions of Organoboron Compounds. *Chem. Rev.* **1995**, *95*, 2457–2483.

(36) Fanta, P. E. The Ullmann Synthesis of Biaryls. *Synthesis* **1974**, *1974*, 9–21.

(37) Djerassi, C. Brominations with N-bromosuccinimide and related compounds; the Wohl-Ziegler reaction. *Chem. Rev.* **1948**, *43*, 271–317.

(38) Platt, E. J.; Wehrly, K.; Kuhmann, S. E.; Chesebro, B.; Kabat, D. Effects of CCR5 and CD4 cell surface concentrations on infections by macrophagetropic isolates of human immunodeficiency virus type 1. *J. Virol.* **1998**, *72*, 2855–2864.

(39) Wei, X.; Decker, J. M.; Liu, H.; Zhang, Z.; Arani, R. B.; Kilby, J. M.; Saag, M. S.; Wu, X.; Shaw, G. M.; Kappes, J. C. Emergence of resistant human immunodeficiency virus type 1 in patients receiving fusion inhibitor (T-20) monotherapy. *Antimicrob. Agents Chemother.* **2002**, *46*, 1896–1905.

(40) Ciminale, V.; Felber, B. K.; Campbell, M.; Pavlakis, G. N. A bioassay for HIV-1 based on Env-CD4 interaction. *AIDS Res. Hum. Retroviruses* **1990**, *6*, 1281–1287.

(41) Popovic, M.; Read-Connole, E.; Gallo, R. C. T4 positive human neoplastic cell lines susceptible to and permissive for HTLV-III. *Lancet* **1984**, *2*, 1472–1473.

(42) Popovic, M. S.; Gartner, E.; Read-Connole, B.; Beaver, M.; Reitz, M. Cell tropism and expression of HIV-1 isolated in natural targets. In *Retroviruses of Human AIDS and Related Animal Diseases*; Valette, L., Girard, M., Eds.; Pasteur Vaccins: Marnes-La-Coquette, France, 1989; pp 219−224.

(43) Ratner, L.; Haseltine, W.; Patarca, R.; Livak, K. J.; Starcich, B.; Josephs, S. F.; Doran, E. R.; Rafalski, J. A.; Whitehorn, E. A.; Baumeister, K.; et al. Complete nucleotide sequence of the AIDS virus, HTLV-III. *Nature* **1985**, *313*, 277–284.

(44) Chackerian, B.; Long, E. M.; Luciw, P. A.; Overbaugh, J. Human immunodeficiency virus type 1 coreceptors participate in postentry stages in the virus replication cycle and function in simian immunodeficiency virus infection. *J. Virol.* **1997**, *71*, 3932–3939.

(45) Morris, G. M.; Huey, R.; Olson, A. J. Using AutoDock for ligand-receptor docking. *Curr. Protoc. Bioinformatics* **2008**, Unit 8.14.